

materials, although a few cases have been reported in heteroepitaxial layers of semiconductors (22, 26). The presence of such defects in semiconductors was rationalized by comparing the energies of complete low-angle tilt grain boundaries with similar disclinations (22). It was shown that the disclinations are energetically more favorable when the misorientations between two crystals is only a few degrees, similar to the rotation in Fig. 2.

The introduction of partial wedge disclinations, dipoles, and other disclination defects into a metal during mechanical milling increases the stored elastic energy (6), as illustrated by the bent planes in Fig. 3. This stored elastic energy may be partly responsible for the unusually high enthalpy, which is on the order of one-third the heat of fusion, that is associated with mechanically milled Fe powder (2). Disclination defects can also contribute to the unusually high strength of fine-grained mechanically milled metals, because the large stress fields associated with them make it difficult for other deformation defects to move through the metal (23, 24). It is also likely that they contribute to the broadening of crystalline peaks in x-ray diffraction patterns commonly observed in mechanically milled metals (12, 14, 28).

The generation and interaction of partial wedge disclinations allows reorientation of crystal volumes only several nanometers in size. This mode of deformation on such a fine scale likely facilitates the fragmentation and reorientation process of metal grains undergoing severe plastic deformation (6, 29), leading to an ultrafine grain size. Thus, partial disclination defects such as those in Fig. 2 can contribute to both the deformation response and the strengthening of metals. The generation of partial disclination defects provides an alternative mechanism to grain boundary sliding, which has been suggested to allow rotation of nanosized crystals during mechanical milling (30). It is not possible to determine exactly how the partial disclination dipoles in Fig. 2 formed from the HRETEM image, although the dislocations likely nucleated at preexisting defects such as grain boundaries or cell walls in the metal (29) and rearranged into the terminating arrays in Fig. 2.

Because HRTEM investigations have been performed on other mechanically milled powders, it is worth commenting why partial disclinations, such as those in Fig. 2, have not been previously reported. One reason for this may be that previous HRTEM investigations were performed on Cu and Cu-Fe alloys, where twinning is a common mode of deformation, and much attention was placed on the formation of twins, shear bands, and grain boundaries, rather than on disclination defects (13, 31). It may also be that the bcc crystal structure of Fe favors the formation of partial disclination defects over other possible types of defects in the material,

and that the high melting temperature of Fe limits movement and annihilation of the defects at ambient temperatures, thereby preserving them in the material for examination. These factors could be tested by performing HRTEM investigations of other high-melting temperature bcc metals and alloys.

We have used HRTEM to directly observe the atomic structure of partial disclination dipoles in bcc Fe that had undergone severe plastic deformation by mechanical milling and shown that the formation and migration of such partial disclinations during deformation allows crystalline solids to rotate and rearrange at the nanometer level. Such rearrangements are important basic phenomena that occur during material deformation, and hence may be critical in the formation of nanocrystalline metals by mechanical milling and other deformation processes. The formation of partial disclination dipoles and other disclination defects facilitates deformation under high stresses, and they also can cause considerable strengthening, owing to the interaction of their elastic stress fields with each other and with grain boundaries in the material. Thus, such disclination defects may make an important contribution to the unique material properties of nanocrystalline metal alloys produced by mechanical milling.

References and Notes

1. J. S. Benjamin, *Metall. Trans.* **1**, 2943 (1970).
2. H. J. Fecht, E. Hellstern, Z. Fu, W. L. Johnson, *Metall. Trans. A21*, 2333 (1990).
3. J. S. C. Jang, C. C. Koch, *Scripta Mater.* **24**, 1599 (1990).
4. Y. Kimura, H. Hidaka, S. Takaki, *Mater. Trans. Jpn. Inst. Met.* **40**, 1149 (1999).
5. H. Gleiter, *Prog. Mater. Sci.* **33**, 233 (1989).
6. A. E. Romanov, V. I. Vladimirov, in *Dislocations in Solids*, vol. 9, *Dislocations and Disclinations*, F. R. N. Nabarro, Ed. (North-Holland, Amsterdam, 1992), pp. 191–402.

7. A. A. Nazarov, A. E. Romanov, R. Z. Valiev, *Scripta Mater.* **34**, 729 (1996).
8. X. Zhu, R. Birringer, U. Herr, H. Gleiter, *Phys. Rev. B* **35**, 9085 (1987).
9. R. W. Siegel, G. J. Thomas, *Ultramicroscopy* **40**, 376 (1992).
10. E. A. Stern, et al., *Phys. Rev. Lett.* **75**, 3874 (1995).
11. J. Schiotz, T. Rasmussen, K. W. Jacobsen, O. H. Nielsen, *Philos. Mag. Lett.* **74**, 339 (1996).
12. Y. H. Zhao, H. W. Sheng, K. Lu., *Acta Mater.* **49**, 365 (2001).
13. J. Y. Huang, Y. K. Wu, H. Q. Ye, *Acta Mater.* **44**, 1211 (1996).
14. A. Revesz, T. Ungar, A. Borbely, J. Lendvai, *Nanostruct. Mater.* **7**, 779 (1996).
15. P. R. Buseck, J. Cowley, L. Eyring, Eds., *High-Resolution Transmission Electron Microscopy and Associated Techniques* (Oxford Univ. Press, Oxford, 1988).
16. G. R. Anstis, J. L. Hutchison, in *Dislocations in Solids*, vol. 9, *Dislocations and Disclinations*, F. R. N. Nabarro, Ed. (North-Holland, Amsterdam, 1992), pp. 1–56.
17. M. Kléman, *Points, Lines and Walls* (Wiley, New York, 1983).
18. S. D. Hudson, *Curr. Opin. Colloid Interface Sci.* **3**, 125 (1998).
19. J. F. Nye, *Proc. R. Soc. A* **387**, 105 (1983).
20. T. W. Chou, H. J. Malasky, *Geophys. Res. B* **84**, 6083 (1979).
21. V. R. Parameswaran, *Specul. Sci. Technol.* **4**, 509 (1979).
22. J. Michler, Y. von Kaenel, J. Stiegler, E. Blank, *J. Appl. Phys.* **83**, 187 (1998).
23. M. J. Marcinkowski, *Philos. Mag.* **36**, 1499 (1977).
24. J. P. Hirth, J. Lothe, *Theory of Dislocations* (McGraw-Hill, New York, 1982).
25. P. M. Wilson, D. C. Martin, *Macromolecules* **29**, 842 (2000).
26. X. Jiang, C. L. Jia, *Appl. Phys. Lett.* **69**, 3902 (1996).
27. Supplementary figures and details of the HRTEM analyses are available on Science Online at www.sciencemag.org/cgi/content/full/295/5564/2433/DC1.
28. K. Zhang, I. V. Alexandrov, R. Z. Valiev, K. Lu, *J. Appl. Phys.* **80**, 5617 (1996).
29. M. Seefeldt, *Rev. Adv. Mater. Sci.* **2**, 44 (2001).
30. J. Schiotz, F. D. Di Tolla, K. W. Jacobsen, *Nature* **391**, 561 (1998).
31. J. Y. Huang, et al., *Acta Mater.* **45**, 113 (1997).
32. We acknowledge the helpful comments of J. P. Hirth and D. C. Martin on this work. Supported by the Ministry of Education, Culture, Sports, Science and Technology of Japan (M.M.) and by the National Science Foundation, Division of Materials Research (grant DMR-9908855) (J.M.H.).

25 October 2001; accepted 19 February 2002

Orbital Influence on Earth's Magnetic Field: 100,000-Year Periodicity in Inclination

Toshitsugu Yamazaki^{1*} and Hirokuni Oda¹

A continuous record of the inclination and intensity of Earth's magnetic field, during the past 2.25 million years, was obtained from a marine sediment core of 42 meters in length. This record reveals the presence of 100,000-year periodicity in inclination and intensity, which suggests that the magnetic field is modulated by orbital eccentricity. The correlation between inclination and intensity shifted from antiphase to in-phase, corresponding to a magnetic polarity change from reversed to normal. To explain the observation, we propose a model in which the strength of the geocentric axial dipole field varies with 100,000-year periodicity, whereas persistent nondipole components do not.

Long-term secular changes in Earth's magnetic field are important for understanding the energy sources of the geodynamo, which

produces the field. Although the geodynamo may be a self-sustained system within Earth's core that is maintained by heat and gravita-

REPORTS

tional energy from the cooling of Earth (1), secular variations with periodicities longer than the electrical diffusion time of the core, which is considered to be about 10,000 years (10 kyrs) (1), may indicate the presence of external energy sources. Previous estimates of the relative strength of the past magnetic field (relative paleointensity) determined from marine sediments (2–5) suggested the occurrence of long-term variations (~10 to 100 kyrs) during the Brunhes Chron (the last 780 kyrs). Some studies have found the Milankovitch orbital frequencies in the paleointensity records [~41-kyr obliquity (6) and ~100-kyr eccentricity (7, 8)] and suggested that orbital forcing or paleoclimate changes energize the geodynamo. Others, however, resulted in contradictory conclusions: They detected no stable frequency (5), or the frequency was an artifact caused by paleoclimatically induced rock-magnetic changes (9–11). Long-period changes are expected to occur in paleomagnetic directions, as well as in intensity, if convection in the liquid outer core is influenced by Earth's orbit or climate. Directional data should be less susceptible to rock-magnetic changes than to paleointensity (9). Previous studies have suggested the presence of long-term directional changes (12–17), but their findings were ambiguous because of the lack of a continuous, long-term record with good age control. Here we present a continuous inclination record during the last 2250 kyrs.

A piston core of 42 m in length (core MD982185) was taken from the West Caroline Basin (WCB) at 3°05.1'N, 134°59.8'E. The water depth of the site is 4415 m. In a previous study in WCB in which cores less than 7 m in length were used, the sediments showed variations in intensity and direction of the magnetic field during the past 200 kyrs (16). The longer core extends the record back to the Matuyama Chron [0.78 to 2.60 million years ago (Ma) (18)]. A total of 1746 discrete samples of 7 cm³ each were taken consecutively from half sections of the core. The core consists mainly of hemipelagic clay, and shows cyclic variations in carbonate content, which reflects glacial-interglacial changes with higher carbonate content in glacial periods. The magnetic susceptibility (*k*) fluctuates as a result of the dilution effect, with lower *k* in glacial periods (Fig. 1A), and these variations in *k* mimic the oxygen isotope ratio ($\delta^{18}\text{O}$) curve (16).

The sediments have stable remanent magnetization throughout the core (19), and the magnetic polarity reversal sequence down to

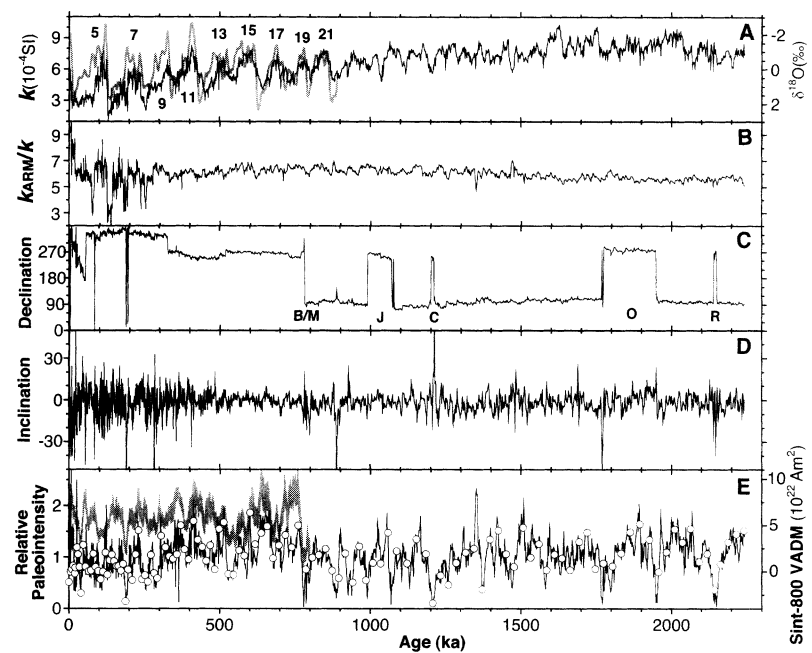


Fig. 1. (A) Volumetric magnetic susceptibility (*k*) (black curve) and reference oxygen isotope ratio ($\delta^{18}\text{O}$) (gray curve) (32) with stage numbers. (B) Ratio of ARM susceptibility to magnetic susceptibility, a parameter testing rock-magnetic homogeneity of the sediments (19). (C) Declinations. The declinations are relative because the core was not azimuthally oriented. Depths in core below the Brunhes-Matuyama boundary [B/M, 780 ka (18)] were converted to ages on the basis of magnetostratigraphy: Jaramillo (J: 990 to 1070 ka), Cobb Mountain (C: 1201 to 1211 ka), Olduvai (O: 1770 to 1950 ka), and Reunion Subchrons (R: 2140 to 2150 ka). Sedimentation rate was assumed to be constant between the polarity boundaries. (D) Inclinations. (E) Relative paleointensity estimated from NRM intensities normalized by ARM (thin black line), and from the "pseudo-Thellier" method (open circles) (19, 28). The age model during the Brunhes Chron was constructed by correlating the relative paleointensity variations to a standard curve, the Sint-800 stack (5) (thick gray line; the origin was shifted for easier comparison between the two). VADM: Virtual axial dipole moment. Tie points were the lows at 40, 110, 190, 290, 390, 530, and 680 ka, and linear interpolation was applied between them.

the Reunion Subchron [2.14 to 2.15 Ma (18)] could be identified from the declination (Fig. 1C). Average inclination is about zero, and thus the polarity sequence cannot be recognized in the inclination (Fig. 1D). An inclination of 6° is expected at the coring site from the hypothetical geocentric axial dipole (GAD), but an inclination anomaly ΔI (20) of -5° to -6° is known to exist in this region (21, 22), which is thought to be caused by persistent nondipole components. The age control of the core is based on the magnetic polarity boundaries at and before the Brunhes/Matuyama (B/M) transition (Fig. 1). The age of the bottom of the core is estimated to be about 2250 kyrs. Within the Brunhes Chron, further constraints were provided by the relative paleointensity variations (presented below) tied to the standard curve Sint-800 (5, 23). The ages based on the relative paleointensity are consistent with those estimated from the *k*- $\delta^{18}\text{O}$ correlation (Fig. 1A). Sedimentation during the Matuyama Chron was almost constant at a rate of about 1.3 cm/kyr, whereas it increased rapidly in the Brunhes Chron and reached 4.9 cm/kyr during the last 190 kyrs [supplementary fig. 1 (19)].

Long-term cyclic changes in the inclination during the past 2250 kyrs are apparent (19). A 100-kyr signal was extracted by means of a band-pass filter centered at this frequency (Fig. 2). A time-series analysis indicates the presence of about 100-kyr periodicity both in the Brunhes and Matuyama Chrons (Fig. 3A). The variation pattern during the last 200 kyrs coincides with the previous record from WCB (16), indicating intercore consistency.

Cyclic lithological changes may induce cyclic changes in the magnitude of the inclination shallowing (24), and then the inclination. However, this cannot explain the inclination variations observed here. In equatorial regions like this site, inclinations are close to zero, and thus inclination shallowing should be negligibly small. Furthermore, the observation that in inclination the 100-kyr periodicity dominates even in the Matuyama Chron, when lithological changes that appeared in the variations of *k* were governed by 40-kyr periodicity (Fig. 3C) (25), excludes the possibility of lithological control on the inclination. Coarse sampling of directional secular variations with 10²- to 10³-year periods could produce apparent long periods by an aliasing effect (26). However, this

¹Institute for Marine Resources and Environment, Geological Survey of Japan, AIST, Tsukuba 305-8567, Japan.

*To whom correspondence should be addressed. E-mail: toshi-yamazaki@aist.go.jp

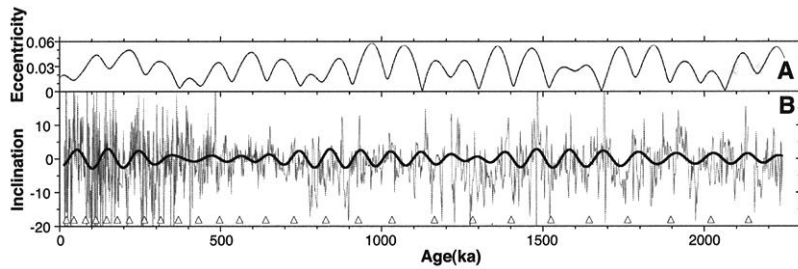


Fig. 2. Long-term secular variations in inclination and orbital eccentricity variations. **(A)** Astronomical solution for orbital eccentricity (33). **(B)** Inclination record, which was subjected to time-series analysis in Fig. 3A (thin lines) (19). The output of a band-pass gaussian filter centered on 0.01 kyr^{-1} (100 kyr) with a band width of 0.002 kyr^{-1} is superimposed (thick curve). Analyseries software (34) was used. Triangles indicate the positions of core-section boundaries at 1.5-m intervals.

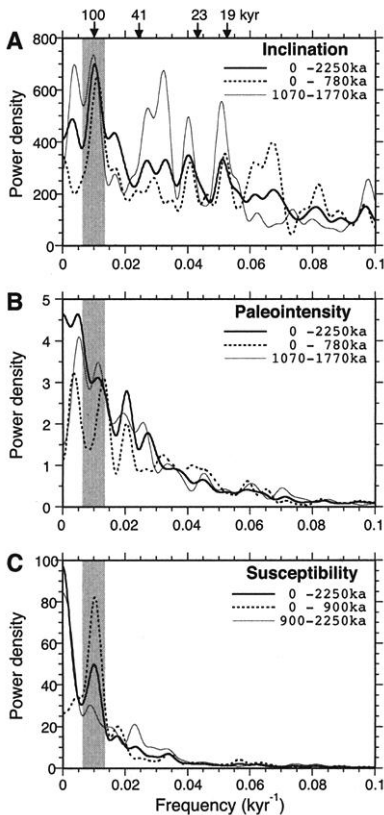


Fig. 3. Power spectrum of **(A)** inclination, **(B)** relative paleointensity, and **(C)** magnetic susceptibility (19). The width of the gray column highlighting a 100-kyr band represents the bandwidth.

cannot explain the observation that the 100-kyr periodicity appears both in the Brunhes and Matuyama Chrons while sampling intervals decrease in the Brunhes Chron because of the increasing sedimentation rate. Smoothing of the variations at postdepositional remanent magnetization (pDRM) acquisition processes (27) should also reduce the aliasing effect. The periodicity is not an artifact caused by sediment deformation when the core was cut into 1.5-m long sections, because the 100-kyr periodicity exists throughout the core despite the upward increase of sedimentation rate [supplementary fig. 1 (19)], and no notable power was observed

at the 1.5-m period. These observations suggest that the 100-kyr periodicity in inclination reflects geomagnetic field behavior. The amplitude of the short-period directional fluctuation is larger in the upper part of the core, at ~ 400 ka and younger, than in the rest of the core (Figs. 1 and 2). This is probably due to a reduced filtering effect on pDRM acquisition (27) caused by the increased sedimentation rate, but one that is not of geomagnetic field origin.

The relative paleointensity is estimated from the natural remanent magnetization (NRM) intensities normalized by anhysteretic remanent magnetization (ARM) (Fig. 1E) (19). The sediments are rock-magnetically homogeneous in general and fulfill the criteria of reliable relative paleointensity determination (2, 19). The relative intensities derived from a normalization by ARM and from the “pseudo-Thellier” method (19, 28) are consistent (Fig. 1E), indicating that the sediments did not suffer seriously from viscous remanent magnetization. The relative paleointensity variations during the Brunhes Chron resemble the standard curve Sint-800 (5), which indicates that our paleointensity record reflects geomagnetic field behavior. A spectral analysis shows the power density at about the 100-kyr period also on the relative paleointensity variations, although it is less dominant than that of the inclination (Fig. 3B). Our record does not show the so-called asymmetric sawtooth pattern, that is, a rapid growth in intensity immediately after a polarity reversal with a gradual decay afterwards (3).

A relation between paleoclimate and occurrence of geomagnetic polarity reversals and excursions has been suggested previously (29, 30); changes in Earth’s moment of inertia caused by paleoclimatically induced ice-volume changes might affect the geodynamo through a core-mantle interaction. The dominance of the 100-kyr signal even when paleoclimate changes were governed by the 40-kyr obliquity period (25) suggests that the long-term secular variations did not result from ice-volume changes. Another important implication of the paleomagnetism is that a time period of longer than 100 yrs is re-

quired for averaging out secular variations, which is much longer than usually assumed, on obtaining, for example, mean virtual geomagnetic pole (VGP) positions for tectonic applications and angular dispersions of VGPs for modeling paleosecular variation.

A cross-correlation analysis between the inclination and paleointensity variations shows a flip of phase relation with the geomagnetic polarity reversal. The phase angle between the two is close to zero during the Brunhes Chron, whereas it is about 180° during the Matuyama Chron [supplementary fig. 2 (19)]. To explain the correlation between inclination and paleointensity, we propose a model in which the strength of the GAD varies with 100-kyr periodicity, whereas those of nondipole components do not vary. Paleodirectional data indicate the presence of persistent nondipole components, which reverse with GAD (22). In WCB, the inclination anomaly ΔI is -5° to -6° (21, 22). In the Brunhes Chron, on the basis of our model, the relative contribution of the nondipole components is expected to be smaller when GAD is stronger, which results in more positive inclinations. When GAD is weaker, more negative inclinations will be observed. The phase angles are thus close to zero. In the Matuyama Chron, the sign of both GAD and the persistent nondipole components are reversed, and thus more negative inclinations are expected at stronger GAD, resulting in phase angles close to 180° . This model is testable; the 100-kyr period in inclination will be obvious where ΔI is large. According to the ΔI map (22), ΔI is large in the east-to-central equatorial Pacific, around Indonesia, and in low latitudes of the Atlantic, and it is small in Eurasia, and in North and South America.

References and Notes

1. R. T. Merrill, M. W. McElhinny, *The Earth’s Magnetic Field* (Academic Press, London, 1983).
2. L. Tauxe, *Rev. Geophys.* **31**, 319 (1993).
3. J.-P. Valet, L. Meynadier, *Nature* **366**, 234 (1993).
4. Y. Guyodo, J.-P. Valet, *Earth Planet. Sci. Lett.* **143**, 23 (1996).
5. ———, *Nature* **399**, 249 (1999).
6. J. E. T. Channell, D. A. Hodell, J. McManus, B. Lehman, *Nature* **394**, 464 (1998).
7. T. Yamazaki, *Earth Planet. Sci. Lett.* **169**, 23 (1999).
8. Y. Yokoyama, T. Yamazaki, *Earth Planet. Sci. Lett.* **181**, 7 (2000).
9. In relative paleointensity estimation, sediments of homogeneous magnetic mineralogy and grain size are used, and differences in the efficiency of the remanent magnetization acquisition of samples, due mainly to differences in magnetic mineral concentration, are normalized, usually by imparting artificial remanent magnetization such as anhysteretic remanent magnetization (ARM) and isothermal remanent magnetization (IRM) (2). At present, however, we cannot exclude the possibility that relative paleointensity estimation is influenced by an unknown rock-magnetic mechanism that amplifies the effects of minor variations in magnetic properties, because the mechanism of remanent magnetization acquisition of sediments is not yet fully understood, and no natural sediments are completely free from lithological variations induced by environmental changes. Determi-

nation of paleomagnetic directions, on the other hand, does not require the normalization of remanent magnetization.

10. Y. Kok, *Earth Planet. Sci. Lett.* **166**, 105 (1999).
11. Y. Guyodo, P. Gaillot, J. E. T. Channell, *Earth Planet. Sci. Lett.* **184**, 109 (2000).
12. R. M. Negrini, K. L. Verosub, J. O. Davis, *Earth Planet. Sci. Lett.* **87**, 173 (1988).
13. K. Creer, N. Thouveny, I. Blunk, *Phys. Earth Planet. Int.* **64**, 314 (1990).
14. S. P. Lund, J. C. Liddicoat, K. R. Lajoie, T. L. Henyey, S. W. Robinson, *Geophys. Res. Lett.* **15**, 1101 (1988).
15. S. Levi, R. Karlin, *Earth Planet. Sci. Lett.* **92**, 219 (1989).
16. T. Yamazaki, N. Ioka, *Earth Planet. Sci. Lett.* **128**, 527 (1994).
17. J. W. Holt, J. L. Kirschvink, F. Garnier, *J. Geophys. Res.* **101**, 11655 (1996).
18. S. C. Cande, D. V. Kent, *J. Geophys. Res.* **100**, 6093 (1995).
19. Supplementary material, presented as a description or figure, is available on Science Online at www.sciencemag.org/cgi/content/full/295/5564/2435/DC1.
20. Inclination anomaly ΔI is defined as observed incli-

nation minus the expected inclination from GAD. Usually, the sign of observed and dipole inclinations within a reversed polarity are inverted to give normal polarity equivalents.

21. D. Gubbins, P. Kelly, *Nature* **365**, 829 (1993).
22. C. L. Johnson, C. G. Constable, *Geophys. J. Int.* **131**, 643 (1997).
23. The Sint-800 paleointensity curve was established by integration of 33 relative paleointensity records from marine sediment cores of various regions. Because the paleointensity variation is globally synchronous, it can be used as a dating tool like the $\delta^{18}\text{O}$ stratigraphy.
24. M. A. Celaya, B. M. Clement, *Geophys. Res. Lett.* **15**, 52 (1988).
25. A major shift in climatic changes from the obliquity to eccentricity periodicities occurred at about 900 ka, which is known as the mid-Pleistocene transition (31). A shift of the dominant frequency in k is observed accordingly in this core. This suggests the validity of the age control in the Matuyama Chron on the basis of magnetostratigraphy.

26. N. Teanby, D. Gubbins, *Geophys. J. Int.* **142**, 563 (2000).
27. M. Hyodo, *J. Geomag. Geoelectr.* **36**, 45 (1984).
28. L. Tauxe, T. Pick, Y. S. Kok, *Geophys. Res. Lett.* **22**, 2885 (1995).
29. M. R. Rampino, *Geology* **7**, 584 (1979).
30. H.-U. Worm, *Earth Planet. Sci. Lett.* **147**, 55 (1997).
31. W. F. Ruddiman, M. E. Raymo, D. G. Martinson, B. M. Clement, J. Backman, *Paleoceanography* **4**, 353 (1989).
32. F. C. Bassinot *et al.*, *Earth Planet. Sci. Lett.* **126**, 91 (1994).
33. J. Laskar, *Icarus* **88**, 266 (1990).
34. D. Paillard, L. Labeyrie, P. Yiou, *EOS* **77**, 379 (1996).
35. We thank E. Usuda for help with the paleomagnetic measurements, Y. Yokoyama for discussion, and the crew and scientists aboard the IMAGES IV cruise for obtaining the core sample, in particular the late Dr. Luejiang Wang. Partly supported by the Superplume Project of the Ministry of Education, Culture, Sports, Science and Technology of Japan.

29 November 2001; accepted 21 February 2002

Sea-Level Fingerprinting as a Direct Test for the Source of Global Meltwater Pulse IA

P. U. Clark,¹ J. X. Mitrovica,^{2*} G. A. Milne,³ M. E. Tamisiea²

The ice reservoir that served as the source for the meltwater pulse IA remains enigmatic and controversial. We show that each of the melting scenarios that have been proposed for the event produces a distinct variation, or fingerprint, in the global distribution of meltwater. We compare sea-level fingerprints associated with various melting scenarios to existing sea-level records from Barbados and the Sunda Shelf and conclude that the southern Laurentide Ice Sheet could not have been the sole source of the meltwater pulse, whereas a substantial contribution from the Antarctic Ice Sheet is consistent with these records.

Records of global sea-level change provide important information on the dynamics and mass balance of glaciers and ice sheets and on the geophysical properties of Earth's interior. Moreover, the sea-level rise from melting ice sheets identifies an increase in the freshwater flux to the ocean that, if targeted at areas of deep water formation, may influence the oceanic thermohaline circulation and cause climate change. Ongoing rates of modern sea-level rise are 1 to 2 mm/year (1). By comparison, the Barbados record of sea-level rise during the last deglaciation identifies an extraordinary event, beginning ~14,200 years before the present (yr B.P.), when rates exceeded 40 mm/year (~20 m over ~500 years) (2), corresponding to a freshwater flux on the order of 0.5 Sv (1 Sv $\equiv 10^6 \text{ m}^3 \text{ s}^{-1}$). This meltwater pulse, mwp-IA, was a period

of exceptionally rapid reduction of the global ice budget, which may have affected atmospheric and ocean circulation through the rapid decrease in ice topography and the large increase in freshwater flux to the ocean. Despite the importance of mwp-IA to the last deglaciation, the specific ice sheets responsible for the event remain uncertain (3). We propose a direct method for establishing the

source of mwp-IA on the basis of geographic variations in the meltwater distribution (or, alternatively, sea-level rise) over the duration of the event.

The Laurentide Ice Sheet is commonly cited as the most likely source of mwp-IA primarily because of its large size (4). Specific evidence suggesting that this ice sheet was responsible for mwp-IA, however, is limited to deep-sea cores from the Gulf of Mexico and the Bermuda Rise that record a decrease in $\delta^{18}\text{O}$ subsequent to the onset of the event (5–8). Insofar as these sites record only meltwater draining through the Mississippi River, interpretation of the isotopic signal as recording mwp-IA necessarily implies that the meltwater pulse originated entirely from the southern sector of the ice sheet: Specifically, the Hudson Strait and Gulf of St. Lawrence also served as outlets for Laurentide meltwater, but records of freshwater flux through these outlets ($\delta^{18}\text{O}$ and ice-rafted debris) indicate insignificant discharge during mwp-IA (9, 10). However, the argument for a lone southern Laurentide source for mwp-IA faces several serious objections (11). The Barents Sea and Fennoscandian Ice

Table 1. Normalized sea-level change for a source of mwp-IA in southern Laurentia. The scenarios "S. Laurentia" and "S. Laurentia-U" refer to cases where the (assumed instantaneous) melting in southern Laurentia is either proportional to ice height at the onset of mwp-IA (as in Fig. 1A) or uniform across the region, respectively. The scenarios "S. Laurentia-M1" and "S. Laurentia-M2" explore the sensitivity of the predictions to variations in the timing of melting. The M1 history assumes that the mwp-IA deglaciation occurred uniformly over a period of 1000 years rather than instantaneously, whereas the M2 history assumes that 20% of the melting took place over the first 400 years, followed by 60% over the next 200 years and the remaining 20% over the last 400 years.

Scenario	Normalized sea-level change					
	Barbados	Sunda Shelf	Tahiti	Bonaparte Gulf	Huon Peninsula	Argentine Shelf
S. Laurentia	0.74	1.12	1.28	1.03	1.08	1.34
S. Laurentia-U	0.74	1.12	1.29	1.04	1.09	1.33
S. Laurentia-M1	0.78	1.11	1.26	1.01	1.06	1.31
S. Laurentia-M2	0.77	1.11	1.26	1.01	1.06	1.31

¹Department of Geosciences, Oregon State University, Corvallis, OR 97331, USA. ²Department of Physics, University of Toronto, Toronto, Ontario M5S 1A7, Canada. ³Department of Geological Sciences, University of Durham, Durham DH1 3LE, UK.

*To whom correspondence should be addressed. E-mail: jxm@physics.utoronto.ca